

# Flower State Classification for Watering System

## DIPLOMARBEIT

zur Erlangung des akademischen Grades

**Diplom-Ingenieur**

im Rahmen des Studiums

**Software Engineering & Internet Computing**

eingereicht von

**Tobias Eidelpes, BSc**

Matrikelnummer 01527193

an der Fakultät für Informatik

der Technischen Universität Wien

Betreuung: Ao.Univ.-Prof. Dr. Horst Eidenberger

Wien, 20. Februar 2023

---

Tobias Eidelpes

---

Horst Eidenberger



# Flower State Classification for Watering System

## DIPLOMA THESIS

submitted in partial fulfillment of the requirements for the degree of

**Diplom-Ingenieur**

in

**Software Engineering & Internet Computing**

by

**Tobias Eidelpes, BSc**

Registration Number 01527193

to the Faculty of Informatics

at the TU Wien

Advisor: Ao.Univ.-Prof. Dr. Horst Eidenberger

Vienna, 20<sup>th</sup> February, 2023

---

Tobias Eidelpes

---

Horst Eidenberger



# **Erklärung zur Verfassung der Arbeit**

Tobias Eidelpes, BSc

Hiermit erkläre ich, dass ich diese Arbeit selbständig verfasst habe, dass ich die verwendeten Quellen und Hilfsmittel vollständig angegeben habe und dass ich die Stellen der Arbeit – einschließlich Tabellen, Karten und Abbildungen –, die anderen Werken oder dem Internet im Wortlaut oder dem Sinn nach entnommen sind, auf jeden Fall unter Angabe der Quelle als Entlehnung kenntlich gemacht habe.

Wien, 20. Februar 2023

---

Tobias Eidelpes



# Danksagung

Ihr Text hier.

---



# Acknowledgements

---

Enter your text here.



# Kurzfassung

---

Ihr Text hier.



# Abstract

---

Enter your text here.



# Contents

<b>Kurzfassung</b>	<b>xi</b>
<b>Abstract</b>	<b>xiii</b>
<b>Contents</b>	<b>xv</b>
<b>1 Introduction</b>	<b>1</b>
1.1 Motivation and Problem Statement . . . . .	1
1.2 Methodological Approach . . . . .	3
1.3 Thesis Structure . . . . .	3
<b>2 Theoretical Background</b>	<b>5</b>
2.1 Related Work . . . . .	5
2.2 Object Detection . . . . .	8
2.3 Classification . . . . .	8
<b>3 Prototype Development</b>	<b>9</b>
3.1 Object Detection . . . . .	9
3.2 Classification . . . . .	9
3.3 Deployment . . . . .	9
<b>4 Results</b>	<b>11</b>
4.1 Object Detection . . . . .	11
4.1.1 Training Phase . . . . .	11
4.1.2 Test Phase . . . . .	13
4.1.3 Hyper-parameter Optimization . . . . .	14
4.2 Classification . . . . .	17
4.2.1 Training Phase . . . . .	18
4.2.2 Hyper-parameter Optimization . . . . .	18
4.2.3 Class Activation Maps . . . . .	22
4.3 Aggregate Model . . . . .	24
4.3.1 Non-optimized Model . . . . .	25
4.3.2 Optimized Model . . . . .	26

<b>List of Figures</b>	<b>29</b>
<b>List of Tables</b>	<b>31</b>
<b>List of Algorithms</b>	<b>33</b>
<b>Acronyms</b>	<b>35</b>
<b>Bibliography</b>	<b>37</b>

# Introduction

Machine learning has seen an unprecedented rise in various research fields during the last few years. Large-scale distributed computing and advances in hardware manufacturing have allowed machine learning models to become more sophisticated and complex. Multi-billion parameter deep learning models show best-in-class performance in Natural Language Processing (NLP) [BMR<sup>+</sup>20], fast object detection [BWL20] and various classification tasks [ZHT22; AH22]. Agriculture is one of the areas which profits substantially from the automation possible with machine learning.

Large-scale as well as small local farmers are able to survey their fields and gardens with drones or stationary cameras to determine soil and plant condition as well as when to water or fertilize [RRL<sup>+</sup>20]. Machine learning models play an important role in that process because they allow automated decision-making in real time.

## 1.1 Motivation and Problem Statement

The challenges to implement an automated system are numerous. First, gathering data in the field requires a network of sensors which are linked to a central server for processing. Since communication between sensors is difficult without proper infrastructure, there is a high demand for processing the data on the sensor itself [MWL22]. Second, differences in local soil, plant and weather conditions require models to be optimized for these diverse inputs. Centrally trained models often lose the nuances present in the data because they have to provide actionable information for a larger area [Awa19]. Third, specialized methods such as hyper- or multispectral imaging in the field provide fine-grained information about the object of interest but come with substantial upfront costs.

To address all of the aforementioned problems, there is a need for an installation which is deployable in the field, gathers data using readily available hardware and performs

## 1. INTRODUCTION

---

computation on the device without a connection to a central server. The device should be able to visually determine whether the plants in its field of view need water or not and output its recommendation.

The aim of this work is to develop a prototype which can be deployed in the field to survey plants and recommend watering or not. To this end, a machine learning model will be trained to first identify the plants in the field of view and then to determine if the plants need water or not. The model should be suitable for edge devices equipped with a TPU or GPU but with otherwise limited processing capabilities. Examples of such systems include Google's Coral development board and the Nvidia Jetson series of single-board computers (SBCs). The model should make use of state-of-the-art algorithms from either classical machine learning or deep learning. The literature review will yield an appropriate machine learning method. Furthermore, the adaption of existing models (transfer learning) for object detection to the domain of plant recognition may provide higher performance than would otherwise be achievable within the time constraints.

The model will be deployed to the single-board computer and evaluated in the field. The evaluation will seek to answer the following questions:

- 1. How well does the model work in theory and how well in practice?*

We will measure the performance of our model with common metrics such as accuracy, F-score, receiver operating characteristics (ROC) curve, and area under curve (AUC). These measurements will allow comparisons between our model and existing models. We expect the plant detection part of the model to achieve high scores on the test dataset. However, the classification of plants into stressed and non-stressed will likely prove to be more difficult. The model is limited to physiological markers of water stress and thus will have difficulties with plants which do not overtly display such features.

Even though models may work well in theory, some do not easily transfer to practical applications. It is, therefore, important to examine if the model is suited for productive use in the field. The evaluation will contain a discussion about the model's transferability because theoretical performance does not automatically guarantee real-world performance due to different environmental conditions.

- 2. What are possible reasons for it to work/not work?*

Even if a model scores high on performance metrics, there might be a mismatch between how researchers think it achieves its goal and how it actually achieves its goal. The results have to be plausible and explainable with its inputs. Otherwise, there can be no confidence in the model's outputs. Conversely, if the model does not work, there must be a reason. We estimate that the curation of the dataset for the training and test phases will play a significant role. Explanations for model out- or underperformance are likely to be found in the structure and composition of the model's inputs.

3. *What are possible improvements to the system in the future?*

The previous two questions will yield the data for possible improvements to the model and/or our approach. With the decision to include a plant detection step at the start, we hope to create consistent conditions for the stress classification. A downside to this approach is that errors during detection can be propagated through the system and result in adverse effects to overall performance. Although we estimate this problem to be negligible, additional feedback regarding our approach in this way might offer insight into potential improvements. If the model does not work as well as expected, which changes to the approach will yield a better result? Similarly to the previous question, the answer will likely lie in the dataset. A heavy focus on dataset construction and curation will ensure satisfactory model performance.

## 1.2 Methodological Approach

The methodological approach consists of the following steps and is also shown in Figure 1.1:

**Literature Review** The literature review informs the type of machine learning methods which are later applied during the implementation of the prototype.

**Object Detection** Flowers present in the image will be detected using object detection methods. These methods will draw bounding boxes around the objects of interest. The output is fed into the next stage.

**State Classification** The bounded images will be fed to a classifier which will determine whether the plant needs water or not.

**Deployment to SBC** The software prototype will be deployed to the single-board computer in the field.

**Evaluation** The prototype will be evaluated in the field to determine its feasibility and performance. During evaluation the author seeks to provide a basis for answering the research questions.

## 1.3 Thesis Structure

The first part of the thesis contains the theoretical basis of the models which we use for the prototype.

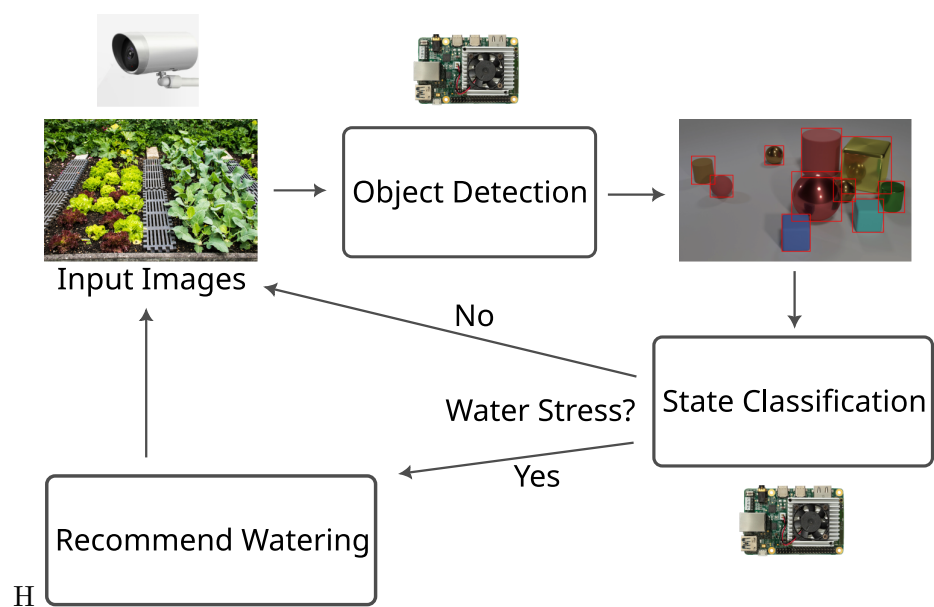


Figure 1.1: Setup in the field for water stress classification.

# CHAPTER 2

## Theoretical Background

Describe the contents of this chapter.

- Related Work. (3 pages)
- Description of inner workings of YOLOv7 as the object detection model. (4 pages)
- Description of inner workings of ResNet as the classification model. (2 pages)

Estimated 9 pages for this chapter.

### 2.1 Related Work

The literature on machine learning in agriculture is broadly divided into four main areas: livestock management, soil management, water management, and crop management [BTD<sup>+</sup>21]. Of those four, water management only makes up about 10% of all surveyed papers during the years 2018–2020. This highlights the potential for research in this area to have a high real-world impact.

Su et al. [SCL<sup>+</sup>20] used traditional feature extraction and pre-processing techniques to train various machine learning models for classifying water stress for a wheat field. They took top-down images of the field using an unmanned aerial vehicle (UAV), segmented wheat pixels from background pixels and constructed features based on spectral intensities and color indices. The features are fed into a support vector machine (SVM) with a Gaussian kernel and optimized using Bayesian optimization. Their results of 92.8% accuracy show that classical machine learning approaches can offer high classification scores if meaningful features are chosen. One disadvantage is that feature extraction is often a tedious task involving trial and error. Advantages are the small dataset and the short training time (3 s) required to obtain a good result.

## 2. THEORETICAL BACKGROUND

---

Similarly, López-García et al. [LIM<sup>+</sup>22] investigated the potential for UAVs to determine water stress for vineyards using RGB and multispectral imaging. The measurements of the UAV were taken at 80m with a common off-the-shelf APS-C sensor. At the same time, stem water measurements were taken with a pressure chamber to be able to evaluate the performance of an artificial neural network (ANN) against the ground truth. The RGB images were used to calculate the green canopy cover (GCC) which was also fed to the model as input. The model achieves a high determination coefficient  $R^2$  of 0.98 for the 2018 season on RGB data with a relative error of  $RE = 10.84\%$ . However, their results do not transfer well to the other seasons under survey (2019 and 2020).

Zhuang et al. [ZWJ<sup>+</sup>17] showed that water stress in maize can be detected early on and, therefore, still provide actionable information before the plants succumb to drought. They installed a camera which took  $640 \times 480$  pixel RGB images every two hours. A simple linear classifier (SVM) segmented the image into foreground and background using the green color channel. The authors constructed a fourteen-dimensional feature space consisting of color and texture features. A gradient boosted decision tree (GBDT) model classified the images into water stressed and non-stressed and achieved an accuracy of 90.39 %. Remarkably, the classification was not significantly impacted by illumination changes throughout the day.

An et al. [ALL<sup>+</sup>19] used the ResNet50 model as a basis for transfer learning and achieved high classification scores (ca. 95%) on maize. Their model was fed with  $640 \times 480$  pixel images of maize from three different viewpoints and across three different growth phases. The images were converted to grayscale which turned out to slightly lower classification accuracy. Their results also highlight the superiority of deep convolutional neural networks (DCNNs) compared to manual feature extraction and gradient boosted decision trees (GBDTs).

Chandel et al. [CCR<sup>+</sup>21] investigated deep learning models in depth by comparing three well-known CNNs. The models under scrutiny were AlexNet, GoogLeNet, and Inception V3. Each model was trained with a dataset containing images of maize, okra, and soybean at different stages of growth and under stress and no stress. The researchers did not include an object detection step before image classification and compiled a fairly small dataset of 1200 images. Of the three models, GoogLeNet beat the other two with a sizable lead at a classification accuracy of >94% for all three types of crop. The authors attribute its success to its inherently deeper structure and application of multiple convolutional layers at different stages. Unfortunately, all of the images were taken at the same  $45^\circ \pm 5^\circ$  angle and it stands to reason that the models would perform significantly worse on images taken under different conditions.

Ramos-Giraldo et al. [RRL<sup>+</sup>20] detected water stress in soybean and corn crops with a pretrained model based on DenseNet-121. Low-cost cameras deployed in the field provided the training data over a 70-day period. They achieved a classification accuracy for the degree of wilting of 88%.

In a later study, the same authors [RRM<sup>+</sup>20] deployed their machine learning model

in the field to test it for production use. They installed multiple Raspberry Pis with attached Raspberry Pi Cameras which took images in 30 min intervals. The authors had difficulties with cameras not working and power supply issues. Furthermore, running the model on the resource-constrained RPis proved difficult and they had to port their TensorFlow model to a TensorFlow Lite model. This conversion lowered their classification scores slightly since it was sometimes off by one water stress level. Nevertheless, their architecture allowed for reasonably high classification scores on corn and soybean with a low-cost setup.

Azimi, Kaur, and Gandhi [AKG20] demonstrate the efficacy of deep learning models versus classical machine learning models on chickpea plants. The authors created their own dataset in a laboratory setting for stressed and non-stressed plants. They acquired 8000 images at eight different angles in total. For the classical machine learning models, they extracted feature vectors using scale-invariant feature transform (SIFT) and histogram of oriented gradients (HOG). The features are fed into three classical machine learning models: support vector machine (SVM), k-nearest neighbors (KNN), and a decision tree (DT) using the classification and regression (CART) algorithm. On the deep learning side, they used their own CNN architecture and the pre-trained ResNet-18 model. The accuracy scores for the classical models was in the range of 60 % to 73 % with the SVM outperforming the two others. The CNN achieved higher scores at 72 % to 78 % and ResNet-18 achieved the highest scores at 82 % to 86 %. The results clearly show the superiority of deep learning over classical machine learning. A downside of their approach lies in the collection of the images. The background in all images was uniformly white and the plants were prominently placed in the center. It should, therefore, not be assumed that the same classification scores can be achieved on plants in the field with messy and noisy backgrounds as well as illumination changes and so forth.

A significant problem in the detection of water stress is posed by the evolution of indicators across time. Since physiological features such as leaf wilting progress as time passes, the additional time domain has to be taken into account. To make use of these spatiotemporal patterns, Azimi, Wadhawan, and Gandhi [AWG21] propose the application of a CNN-long short-term memory (CNN-LSTM) architecture. The model was trained on chickpea plants and achieves a robust classification accuracy of >97%.

All of the previously mentioned studies solely focus on either one specific type of plant or on a small number of them. Furthermore, the researchers construct their datasets in homogeneous environments which often do not mimic real-world conditions. Finally, there exist no studies on common household or garden plants. This fact may be attributed to the propensity for funding to come from the agricultural sector. It is thus desirable to explore how plants other than crops show water stress and if there is additional information to be gained from them.

## 2.2 Object Detection

Describe the inner workings of the YOLOv7 model structure. Reference the original paper [WBL22] and possibly papers of previous versions of the same model (YOLOv5 [JCS<sup>+</sup>22], YOLOv4 [BWL20]).

Estimated 4 pages for this section.

## 2.3 Classification

Describe the inner workings of the ResNet model structure. Reference the original paper [HZR<sup>+</sup>16].

Estimated 2 pages for this section.

# CHAPTER 3

## Prototype Development

Describe the architecture of the prototype regarding the overall design, how the object detection model was trained and tuned, and do the same for the classifier. Also describe the shape and contents of the training sets.

### 3.1 Object Detection

Describe how the object detection model was trained, what the training set looks like and which complications arose during training as well as fine-tuning.

### 3.2 Classification

Describe how the classification model was trained, what the training set looks like and which complications arose during training as well as fine-tuning.

### 3.3 Deployment

Describe the Jetson Nano, how the model is deployed to the device and how it reports its results.



# Results

The following sections contain a detailed evaluation of the model in various scenarios. First, we present metrics from the training phases of the constituent models. Second, we employ methods from the field of Explainable Artificial Intelligence (XAI) such as Gradient-weighted Class Activation Mapping (Grad-CAM) to get a better understanding of the models' abstractions. Finally, we turn to the models' aggregate performance on the test set.

## 4.1 Object Detection

The object detection model was pre-trained on the COCO [LMB<sup>+</sup>15] dataset and fine-tuned with data from the Open Images Dataset (OID) [KRA<sup>+</sup>20] in its sixth version. Since the full OID dataset contains considerably more classes and samples than would be feasibly trainable on a small cluster of GPUs, only images from the two classes *Plant* and *Houseplant* have been downloaded. The samples from the Houseplant class are merged into the Plant class because the distinction between the two is not necessary for our model. Furthermore, the OID contains not only bounding box annotations for object detection tasks, but also instance segmentations, classification labels and more. These are not needed for our purposes and are omitted as well. In total, the dataset consists of 91479 images with a roughly 85/5/10 split for training, validation and testing, respectively.

### 4.1.1 Training Phase

The object detection model was trained for 300 epochs on 79204 images with 284130 ground truth labels. The weights from the best-performing epoch were saved. The model's fitness for each epoch is calculated as the weighted average of mAP@0.5 and mAP@0.5:0.95:

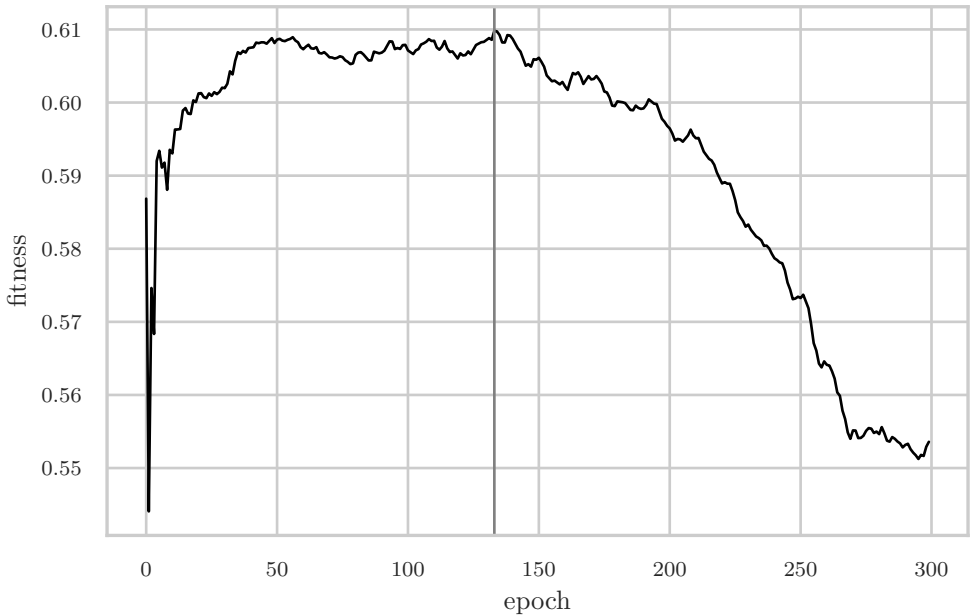


Figure 4.1: Object detection model fitness for each epoch calculated as in equation 4.1. The vertical gray line at 133 marks the epoch with the highest fitness.

$$f_{epoch} = 0.1 \cdot \text{mAP}@0.5 + 0.9 \cdot \text{mAP}@0.5:0.95 \quad (4.1)$$

Figure 4.1 shows the model’s fitness over the training period of 300 epochs. The gray vertical line indicates the maximum fitness of 0.61 at epoch 133. The weights of that epoch were frozen to be the final model parameters. Since the fitness metric assigns the mAP at the higher range the overwhelming weight, the mAP@0.5 starts to decrease after epoch 30, but the mAP@0.5:0.95 picks up the slack until the maximum fitness at epoch 133. This is an indication that the model achieves good performance early on and continues to gain higher confidence values until performance deteriorates due to overfitting.

Overall precision and recall per epoch are shown in figure 4.2. The values indicate that neither precision nor recall change materially during training. In fact, precision starts to decrease from the beginning, while recall experiences a barely noticeable increase. Taken together with the box and object loss from figure 4.3, we speculate that the pre-trained model already generalizes well to plant detection because one of the categories in the COCO [LMB<sup>+</sup>15] dataset is *potted plant*. Any further training solely impacts the confidence of detection, but does not lead to higher detection rates. This conclusion is supported by the increasing mAP@0.5:0.95 until epoch 133.

Further culprits for the flat precision and recall values may be found in bad ground truth data. The labels from the OID are sometimes not fine-grained enough. Images

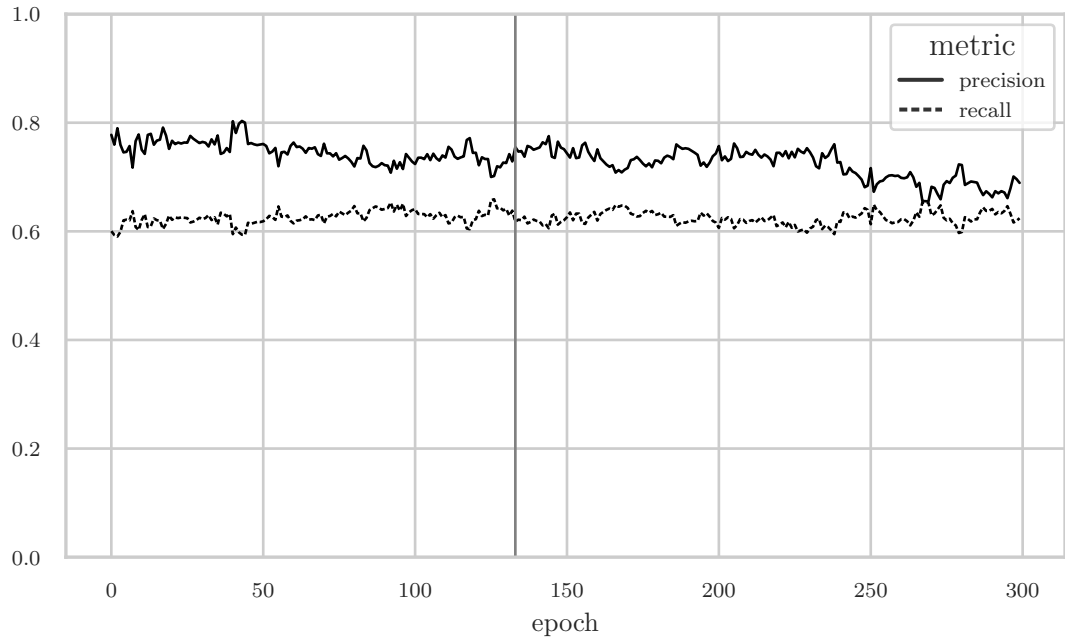


Figure 4.2: Overall precision and recall during training for each epoch. The vertical gray line at 133 marks the epoch with the highest fitness.

which contain multiple individual—often overlapping—plants are labeled with one large bounding box instead of multiple smaller ones. The model recognizes the individual plants and returns tighter bounding boxes even if that is not what is specified in the ground truth. Therefore, it is prudent to limit the training phase to relatively few epochs in order to not penalize the more accurate detections of the model. The smaller bounding boxes make more sense considering the fact that the cutout is passed to the classifier in a later stage. Smaller bounding boxes help the classifier to only focus on one plant at a time and to not get distracted by multiple plants in potentially different stages of wilting.

The box loss decreases slightly during training which indicates that the bounding boxes become tighter around objects of interest. With increasing training time, however, the object loss increases, indicating that less and less plants are present in the predicted bounding boxes. It is likely that overfitting is a cause for the increasing object loss from epoch 40 onward. Since the best weights as measured by fitness are found at epoch 133 and the object loss accelerates from that point, epoch 133 is probably the correct cutoff before overfitting occurs.

### 4.1.2 Test Phase

Of the 91479 images around 10% were used for the test phase. These images contain a total of 12238 ground truth labels. Table 4.1 shows precision, recall and the harmonic mean of both (F1-score). The results indicate that the model errs on the side of sensitivity

## 4. RESULTS

---

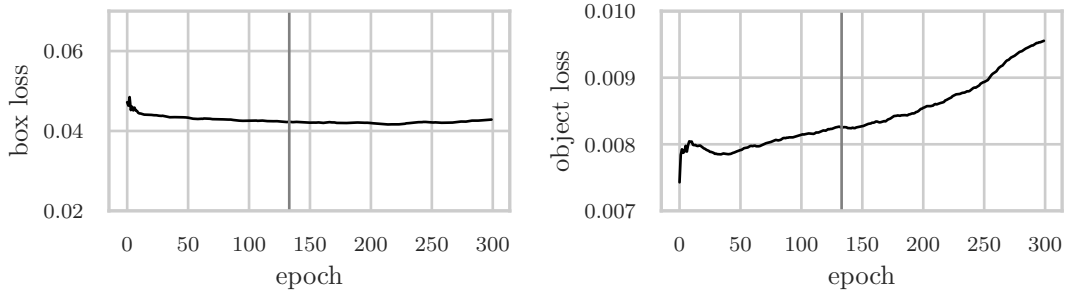


Figure 4.3: Box and object loss measured against the validation set of 3091 images and 4092 ground truth labels. The class loss is omitted because there is only one class in the dataset and the loss is therefore always zero.

because recall is higher than precision. Although some detections are not labeled as plants in the dataset, if there is a labeled plant in the ground truth data, the chance is high that it will be detected. This behavior is in line with how the model’s detections are handled in practice. The detections are drawn on the original image and the user is able to check the bounding boxes visually. If there are wrong detections, the user can ignore them and focus on the relevant ones instead. A higher recall will thus serve the user’s needs better than a high precision.

	Precision	Recall	F1-score	Support
Plant	0.547571	0.737866	0.628633	12238.0

Table 4.1: Precision, recall and F1-score for the object detection model.

Figure 4.4 shows the Average Precision (AP) for the Intersection over Union (IOU) thresholds of 0.5 and 0.95. Predicted bounding boxes with an IOU of less than 0.5 are not taken into account for the precision and recall values of table 4.1. The lower the detection threshold, the more plants are detected. Conversely, a higher detection threshold leaves potential plants undetected. The precision-recall curves confirm this behavior because the area under the curve for the threshold of 0.5 is higher than for the threshold of 0.95 (0.66 versus 0.41). These values are combined in COCO’s [LMB<sup>+</sup>15] main evaluation metric which is the AP averaged across the IOU thresholds from 0.5 to 0.95 in 0.05 steps. This value is then averaged across all classes and called mean average precision (mAP). The object detection model achieves a state-of-the-art mAP of 0.5727 for the *Plant* class.

### 4.1.3 Hyper-parameter Optimization

To further improve the object detection performance, we perform hyper-parameter optimization using a genetic algorithm. Evolution of the hyper-parameters starts from the initial 30 default values provided by the authors of YOLO. Of those 30 values, 26 are allowed to mutate. During each generation, there is an 80% chance that a mutation

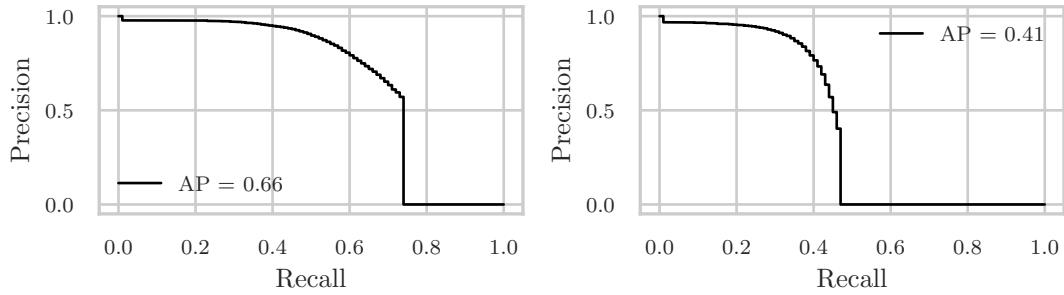


Figure 4.4: Precision-recall curves for IOU thresholds of 0.5 and 0.95. The AP of a specific threshold is defined as the area under the precision-recall curve of that threshold. The mAP across IOU thresholds from 0.5 to 0.95 in 0.05 steps  $\text{mAP}@0.5:0.95$  is 0.5727.

occurs with a variance of 0.04. To determine which generation should be the parent of the new mutation, all previous generations are ordered by fitness in decreasing order. At most five top generations are selected and one of them is chosen at random. Better generations have a higher chance of being selected as the selection is weighted by fitness. The parameters of that chosen generation are then mutated with the aforementioned probability and variance. Each generation is trained for three epochs and the fitness of the best epoch is recorded.

In total, we ran 87 iterations of which the 34<sup>th</sup> generation provides the best fitness of 0.6076. Due to time constraints, it was not possible to train each generation for more epochs or to run more iterations in total. We assume that the performance of the first few epochs is a reasonable proxy for model performance overall. The optimized version of the object detection model is then trained for 70 epochs using the parameters of the 34<sup>th</sup> generation.

Figure 4.5 shows the model’s fitness during training for each epoch. After the highest fitness of 0.6172 at epoch 27, the performance quickly declines and shows that further training would likely not yield improved results. The model converges to its highest fitness much earlier than the non-optimized version, which indicates that the adjusted parameters provide a better starting point in general. Furthermore, the maximum fitness is 0.74% higher than in the non-optimized version.

Figure 4.6 shows precision and recall for the optimized model during training. Similarly to the non-optimized model from figure 4.2, both metrics do not change materially during training. Precision is slightly higher than in the non-optimized version and recall hovers at the same levels.

The box and object loss during training is pictured in figure 4.7. Both losses start from a lower level which suggests that the initial optimized parameters allow the model to converge quicker. The object loss exhibits a similar slope to the non-optimized model in figure 4.3. The vertical gray line again marks epoch 27 with the highest fitness. The box

## 4. RESULTS

---

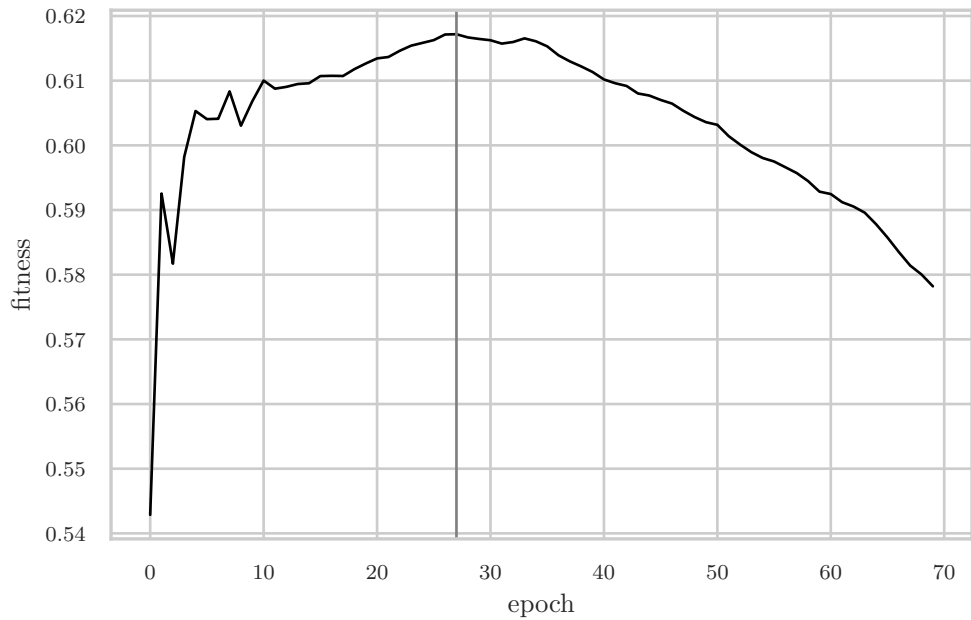


Figure 4.5: Object detection model fitness for each epoch calculated as in equation 4.1. The vertical gray line at 27 marks the epoch with the highest fitness of 0.6172.

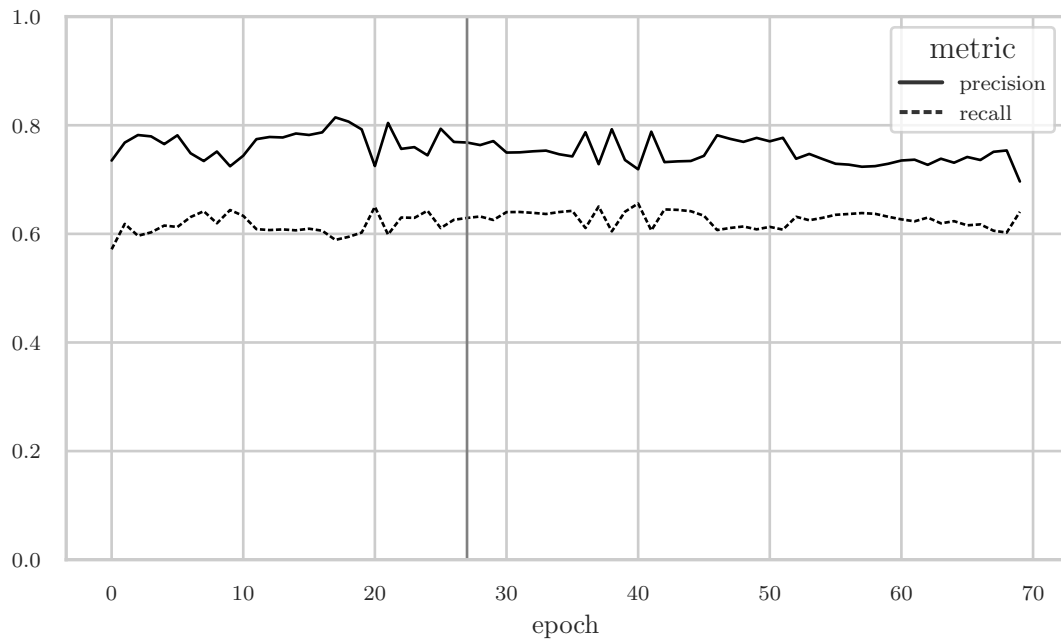


Figure 4.6: Overall precision and recall during training for each epoch of the optimized model. The vertical gray line at 27 marks the epoch with the highest fitness.

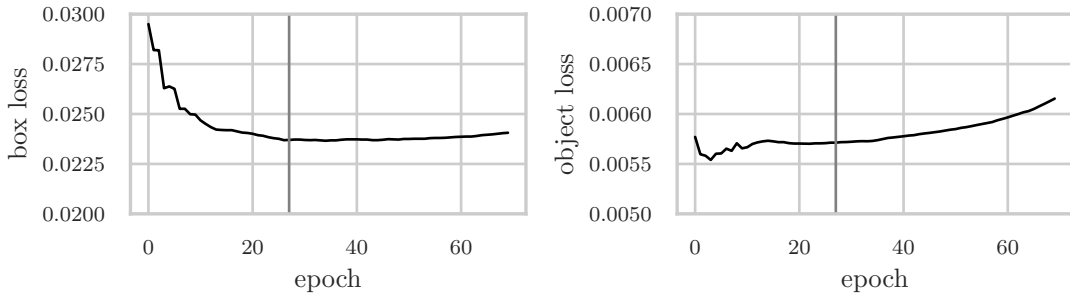


Figure 4.7: Box and object loss measured against the validation set of 3091 images and 4092 ground truth labels. The class loss is omitted because there is only one class in the dataset and the loss is therefore always zero.

loss reaches its lower limit at that point and the object loss starts to increase again after epoch 27.

	Precision	Recall	F1-score	Support
Plant	0.633358	0.702811	0.666279	12238.0

Table 4.2: Precision, recall and F1-score for the optimized object detection model.

Turning to the evaluation of the optimized model on the test dataset, table 4.2 shows precision, recall and the F1-score for the optimized model. Comparing these metrics with the non-optimized version from table 4.1, precision is significantly higher by more than 8.5%. Recall, however, is 3.5% lower. The F1-score is higher by more than 3.7% which indicates that the optimized model is better overall despite the lower recall. We feel that the lower recall value is a suitable trade off for the substantially higher precision considering that the non-optimized model's precision is quite low at 0.55.

The precision-recall curves in figure 4.8 for the optimized model show that the model draws looser bounding boxes than the optimized model. The AP for both IOU thresholds of 0.5 and 0.95 is lower indicating worse performance. It is likely that more iterations during evolution would help increase the AP values as well. Even though the precision and recall values from table 4.2 are better, the mAP@0.5:0.95 is lower by 1.8%.

## 4.2 Classification

The classifier receives cutouts from the object detection model and determines whether the image shows a stressed plant or not. To achieve this goal, we trained a Residual Neural Network (ResNet) [HZR<sup>+</sup>16] on a dataset of 452 images of healthy and 452 stressed plants. We chose the ResNet architecture due to its popularity and ease of implementation as well as its consistently high performance on various classification tasks. While its classification speed in comparison with networks optimized for mobile and edge

## 4. RESULTS

---

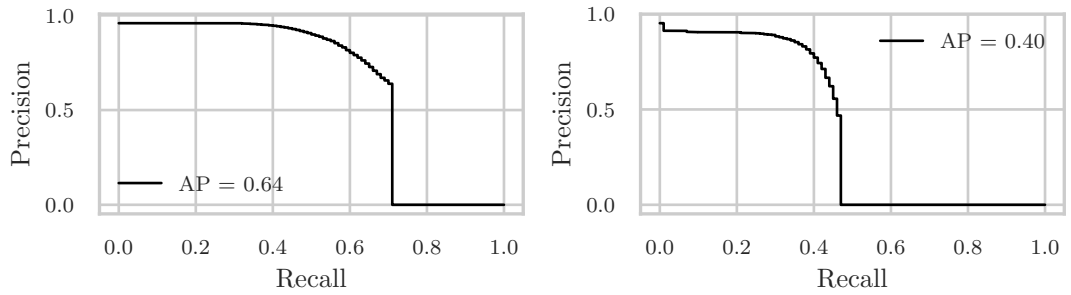


Figure 4.8: Precision-recall curves for IOU thresholds of 0.5 and 0.95. The AP of a specific threshold is defined as the area under the precision-recall curve of that threshold. The mAP across IOU thresholds from 0.5 to 0.95 in 0.05 steps mAP@0.5:0.95 is 0.5546.

devices (e.g. MobileNet) is significantly lower, the deeper structure and the additional parameters are necessary for the fairly complex task at hand. Furthermore, the generous time budget for object detection *and* classification allows for more accurate results at the expense of speed. The architecture allows for multiple different structures, depending on the amount of layers. The smallest one has 18 and the largest 152 layers with 34, 50 and 101 in-between. The larger networks have better accuracy in general, but come with trade-offs regarding training and inference time as well as required space. The 50 layer architecture (ResNet50) is adequate for our use case.

### 4.2.1 Training Phase

The dataset was split 85/15 into training and validation sets. The images in the training set were augmented with a random crop to arrive at the expected image dimensions of 224 pixels. Additionally, the training images were modified with a random horizontal flip to increase the variation in the set and to train a rotation invariant classifier. All images, regardless of their membership in the training or validation set, were normalized with the mean and standard deviation of the ImageNet [DDS<sup>+</sup>09] dataset, which the original ResNet model was pre-trained with. Training was done for 50 epochs and the best-performing model as measured by validation accuracy was selected as the final version.

Figure 4.9 shows accuracy and loss on the training and validation sets. There is a clear upwards trend until epoch 20 when validation accuracy and loss stabilize at around 0.84 and 0.3, respectively. The quick convergence and resistance to overfitting can be attributed to the model already having robust feature extraction capabilities.

### 4.2.2 Hyper-parameter Optimization

In order to improve the aforementioned accuracy values, we perform hyper-parameter optimization across a wide range of parameters. Table 4.3 lists the hyper-parameters and their possible values. Since the number of all combinations of values is 11520 and

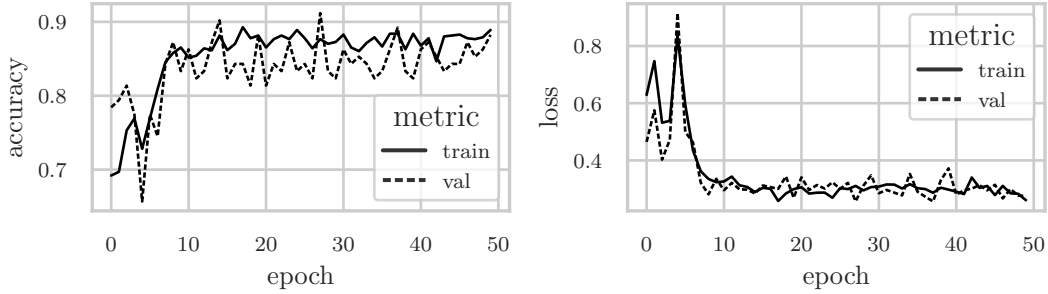


Figure 4.9: Accuracy and loss during training of the classifier. The model converges quickly, but additional epochs do not cause validation loss to increase, which would indicate overfitting. The maximum validation accuracy of 0.9118 is achieved at epoch 27.

each combination is trained for 10 epochs with a training time of approximately six minutes per combination, exhausting the search space would take 48 days. Due to time limitations, we have chosen to not search exhaustively but to pick random combinations instead. Random search works surprisingly well—especially compared to grid search—in a number of domains, one of which is hyper-parameter optimization [BB12].

Parameter	Values
optimizer	adam, sgd
batch size	4, 8, 16, 32, 64
learning rate	0.0001, 0.0003, 0.001, 0.003, 0.01, 0.1
step size	2, 3, 5, 7
gamma	0.1, 0.5
beta one	0.9, 0.99
beta two	0.5, 0.9, 0.99, 0.999
eps	0.00000001, 0.1, 1

Table 4.3: Hyper-parameters and their possible values during optimization.

The random search was run for 138 iterations which equates to a 75% probability that the best solution lies within 1% of the theoretical maximum (4.2). Figure 4.10 shows three of the eight parameters and their impact on a high F1-score. Stochastic Gradient Descent (SGD) has less variation in its results than Adam [KB17] and manages to provide eight out of the ten best results. The number of epochs to train for was chosen based on the observation that almost all configurations converge well before reaching the tenth epoch. The assumption that a training run with ten epochs provides a good proxy for final performance is supported by the quick convergence of validation accuracy and loss in figure 4.9.

$$1 - (1 - 0.01)^{138} \approx 0.75 \quad (4.2)$$

## 4. RESULTS

---

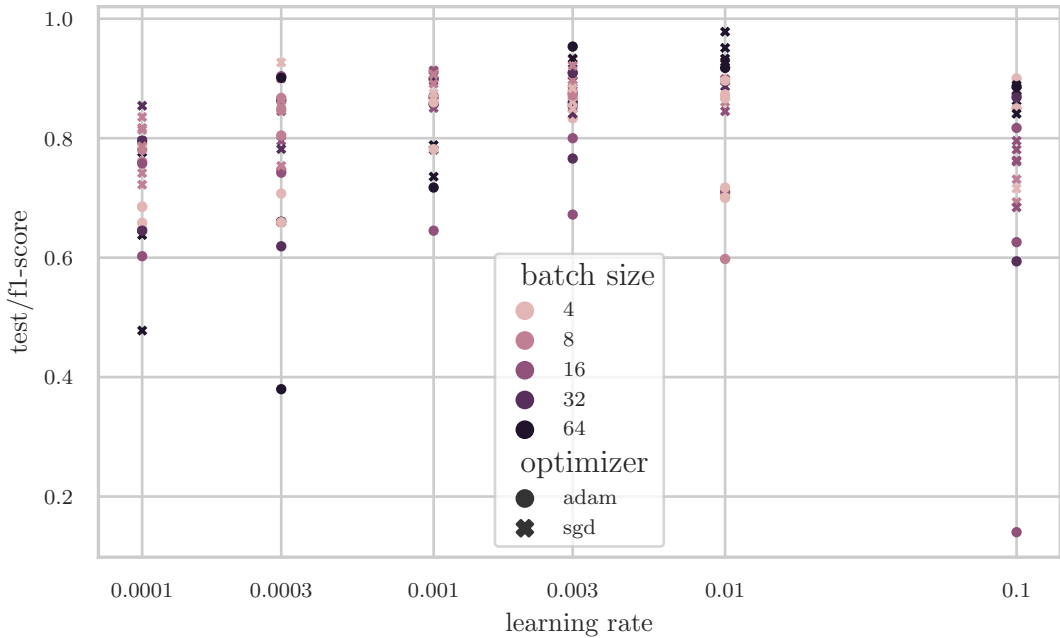


Figure 4.10: This figure shows three of the eight hyper-parameters and their performance measured by the F1-score during 138 trials. Differently colored markers show the batch size with darker colors representing a larger batch size. The type of marker (circle or cross) shows which optimizer was used. The x-axis shows the learning rate on a logarithmic scale. In general, a learning rate between 0.003 and 0.01 results in more robust and better F1-scores. Larger batch sizes more often lead to better performance as well. As for the type of optimizer, SGD produced the best iteration with an F1-score of 0.9783. Adam tends to require more customization of its parameters than SGD to achieve good results.

Table 4.4 lists the final hyper-parameters which were chosen to train the improved model. In order to confirm that the model does not suffer from overfitting or is a product of chance due to a coincidentally advantageous train/test split, we perform stratified 10-fold cross validation on the dataset. Each fold contains 90% training and 10% test data and was trained for 25 epochs. Figure 4.11 shows the performance of the epoch with the highest F1-score of each fold as measured against the test split. The mean Receiver Operating Characteristic (ROC) curve provides a robust metric for a classifier's performance because it averages out the variability of the evaluation. Each fold manages to achieve at least an Area Under the Curve (AUC) of 0.94, while the best fold reaches 0.98. The mean ROC has an AUC of 0.96 with a standard deviation of 0.02. These results indicate that the model is accurately predicting the correct class and is robust against variations in the training set.

The classifier shows good performance so far, but care has to be taken to not overfit the model to the training set. Comparing the F1-score during training with the F1-score

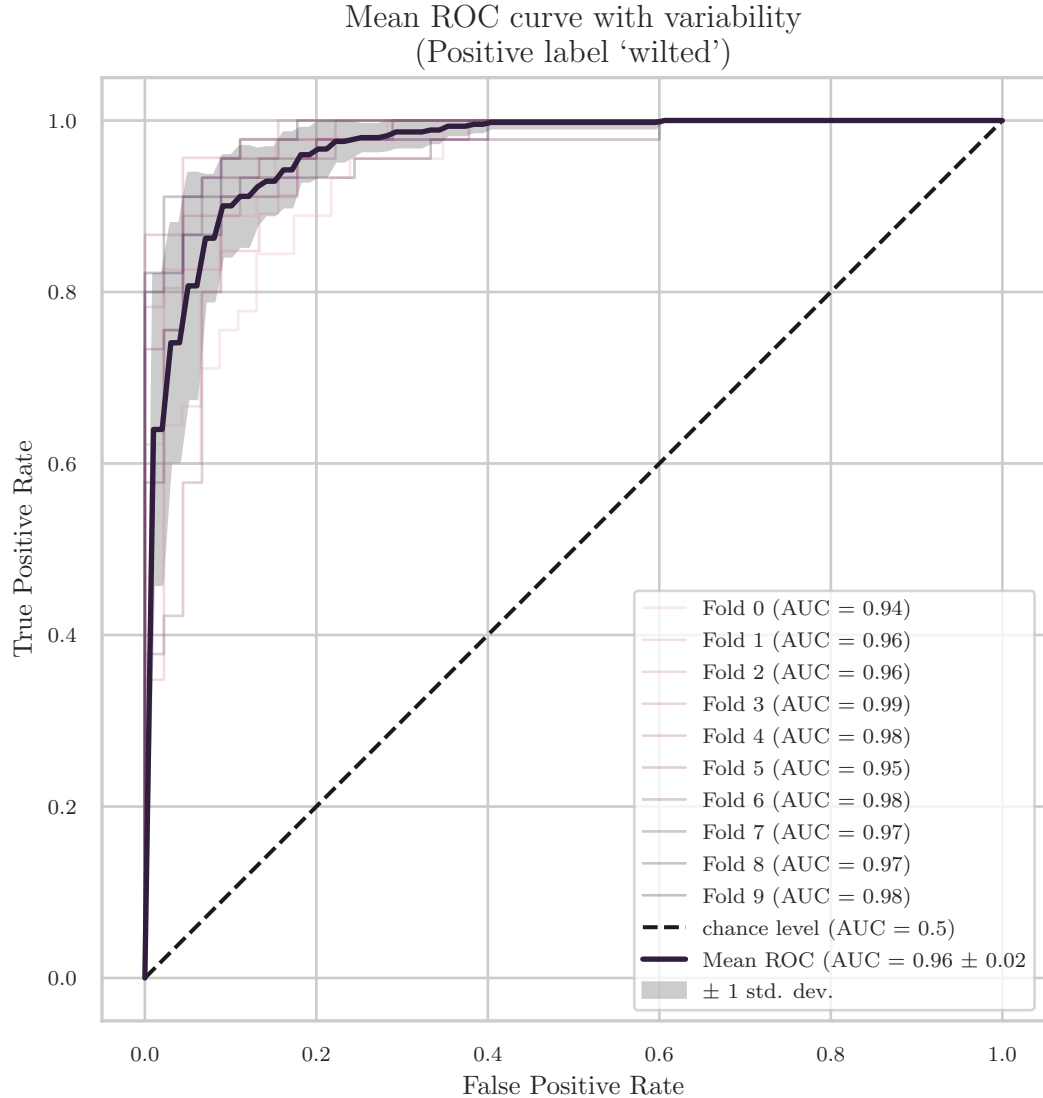


Figure 4.11: This plot shows the ROC curve for the epoch with the highest F1-score of each fold as well as the AUC. To get a less variable performance metric of the classifier, the mean ROC curve is shown as a thick line and the variability is shown in gray. The overall mean AUC is 0.96 with a standard deviation of 0.02. The best-performing fold reaches an AUC of 0.99 and the worst an AUC of 0.94. The black dashed line indicates the performance of a classifier which picks classes at random (AUC = 0.5). The shapes of the ROC curves show that the classifier performs well and is robust against variations in the training set.

Optimizer	Batch Size	Learning Rate	Step Size
SGD	64	0.01	5

Table 4.4: Chosen hyper-parameters for the final, improved model. The difference to the parameters listed in Table 4.3 comes as a result of choosing SGD over Adam. The missing four parameters are only required for Adam and not SGD.

during testing gives insight into when the model tries to increase its performance during training at the expense of generalizability. Figure 4.12 shows the F1-scores of each epoch and fold. The classifier converges quickly to 1 for the training set at which point it experiences a slight drop in generalizability. Training the model for at most five epochs is sufficient because there are generally no improvements afterwards. The best-performing epoch for each fold is between the second and fourth epoch which is just before the model achieves an F1-score of 1 on the training set.

#### 4.2.3 Class Activation Maps

Neural networks are notorious for their black-box behavior, where it is possible to observe the inputs and the corresponding outputs, but the stage in-between stays hidden from view. Models are continuously developed and deployed to aid in human decision-making and sometimes supplant it. It is, therefore, crucial to obtain some amount of interpretability of what the model does *inside* to be able to explain why a decision was made in a certain way. The research field of XAI gained significance during the last few years because of the development of new methods to peek inside these black boxes.

One such method, Class Activation Mapping (CAM) [ZKL<sup>+</sup>15], is a popular tool to produce visual explanations for decisions made by Convolutional Neural Networks (CNNs). Convolutional layers essentially function as object detectors as long as no fully-connected layers perform the classification. This ability to localize regions of interest, which play a significant role in the type of class the model predicts, can be retained until the last layer and used to generate activation maps for the predictions.

A more recent approach to generating a CAM via gradients is proposed by Selvaraju et al. [SCD<sup>+</sup>20]. Their Grad-CAM approach works by computing the gradient of the feature maps of the last convolutional layer with respect to the specified class. The last layer is chosen because the authors find that “[...] Grad-CAM maps become progressively worse as we move to earlier convolutional layers as they have smaller receptive fields and only focus on less semantic local features.” [SCD<sup>+</sup>20, p.5]

Turning to our classifier, figure 4.13 shows the CAMs for *healthy* and *stressed*. While the regions of interest for the *healthy* class lie on the healthy plant, the *stressed* plant is barely considered and mostly rendered as background information (blue). Conversely, when asked to explain the inputs to the *stressed* classification, the regions of interest predominantly stay on the thirsty as opposed to the healthy plant. In fact, the large

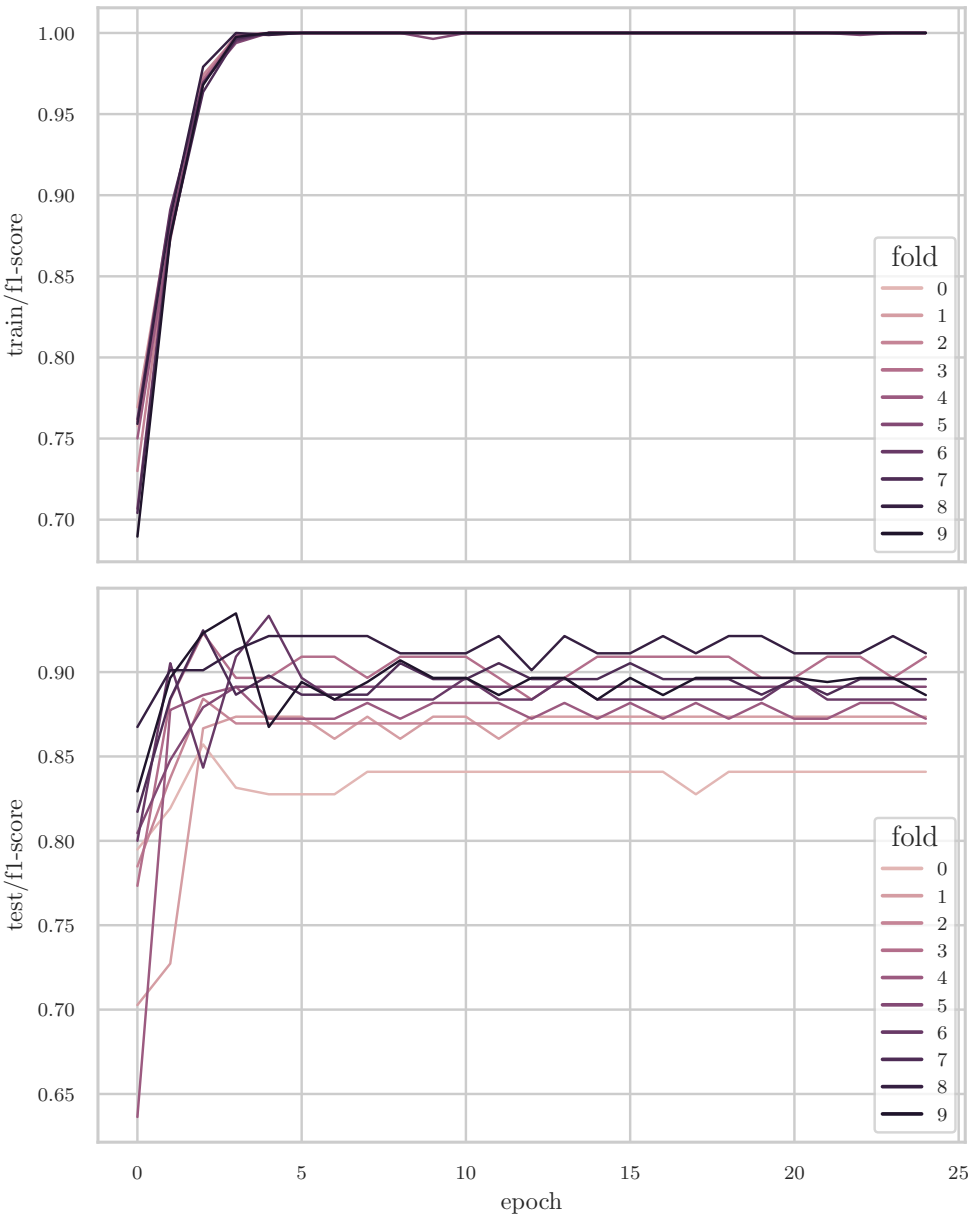


Figure 4.12: These plots show the F1-score during training as well as testing for each of the folds. The classifier converges to 1 by the third epoch during the training phase, which might indicate overfitting. However, the performance during testing increases until epoch three in most cases and then stabilizes at approximately 2-3% lower than the best epoch. We believe that the third, or in some cases fourth, epoch is detrimental to performance and results in overfitting, because the model achieves an F1-score of 1 for the training set, but that gain does not transfer to the test set. Early stopping during training alleviates this problem.

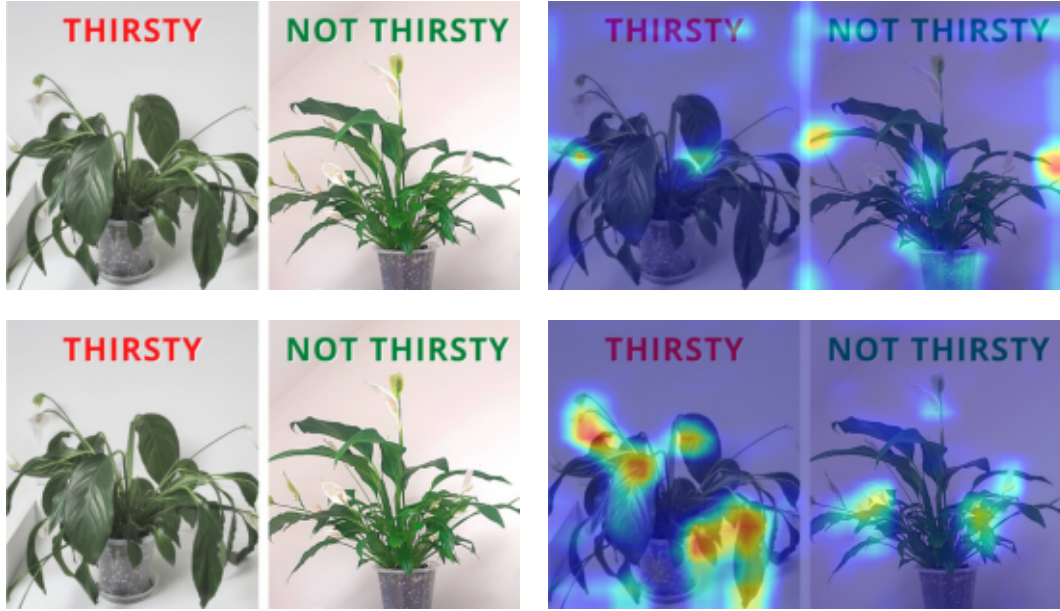


Figure 4.13: The top left image shows the original image of the same plant in a stressed (left) and healthy (right) state. In the top right image, the CAM for the class *healthy* is laid over the original image. The classifier draws its conclusion mainly from the healthy plant, which is indicated by the red hot spots around the tips of the plant. The bottom right image shows the CAM for the *stressed* class. The classifier focuses on the hanging leaves of the thirsty plant. The image was classified as *stressed* with a confidence of 70%.

hanging leaves play a significant role in determining the class the image belongs to. This is an additional data point confirming that the model focuses on the semantically meaningful parts of the image during classification.

### 4.3 Aggregate Model

In this section we turn to the evaluation of the aggregate model. We have confirmed the performance of the constituent models: the object detection and the classification model. It remains to evaluate the complete pipeline from gathering detections of potential plants in an image and forwarding them to the classifier to obtaining the results as either healthy or stressed with their associated confidence scores.

The test set contains 640 images which were obtained from a google search using the terms *thirsty plant*, *wilted plant* and *stressed plant*. Images which clearly show one or multiple plants with some amount of visible stress were added to the dataset. Care was taken to include plants with various degrees of stress and in various locations and lighting conditions. The search not only provided images of stressed plants, but also of healthy plants due to articles, which describe how to care for plants, having a banner image of

	precision	recall	f1-score	support
Healthy	0.665	0.554	0.604	766
Stressed	0.639	0.502	0.562	494
micro avg	0.655	0.533	0.588	1260
macro avg	0.652	0.528	0.583	1260
weighted avg	0.655	0.533	0.588	1260

Table 4.5: Precision, recall and F1-score for the aggregate model.

healthy plants. The dataset is biased towards potted plants which are commonly put on display in western households. Furthermore, many plants, such as succulents, are sought after for home environments because of their ease of maintenance. Due to their inclusion in the dataset and how they exhibit water stress, the test set nevertheless contains a wide variety of scenarios.

After collecting the images, the aggregate model was run on them to obtain initial bounding boxes and classifications for ground truth labeling. Letting the model do the work beforehand and then correcting the labels allowed to include more images in the test set because they could be labeled more easily. Additionally, going over the detections and classifications provided a comprehensive view on how the models work and what their weaknesses and strengths are. After the labels have been corrected, the ground truth of the test set contains 766 bounding boxes of healthy plants and 494 of stressed plants.

### 4.3.1 Non-optimized Model

Table 4.5 shows precision, recall and the F1-score for both classes *Healthy* and *Stressed*. Precision is higher than recall for both classes and the F1-score is at 0.59. Unfortunately, these values do not take the accuracy of bounding boxes into account and thus have only limited expressive power.

Figure 4.14 shows the precision and recall curves for both classes at different IOU thresholds. The left plot shows the AP for each class at the threshold of 0.5 and the right one at 0.95. The mAP is 0.3581 and calculated across all classes as the median of the IOU thresholds from 0.5 to 0.95 in 0.05 steps. The cliffs at around 0.6 (left) and 0.3 (right) happen at a detection threshold of 0.5. The classifier's last layer is a softmax layer which necessarily transforms the input into a probability of showing either a healthy or stressed plant. If the probability of an image showing a healthy plant is below 0.5, it is no longer classified as healthy but as stressed. The threshold for discriminating the two classes lies at the 0.5 value and is therefore the cutoff for either class.

## 4. RESULTS

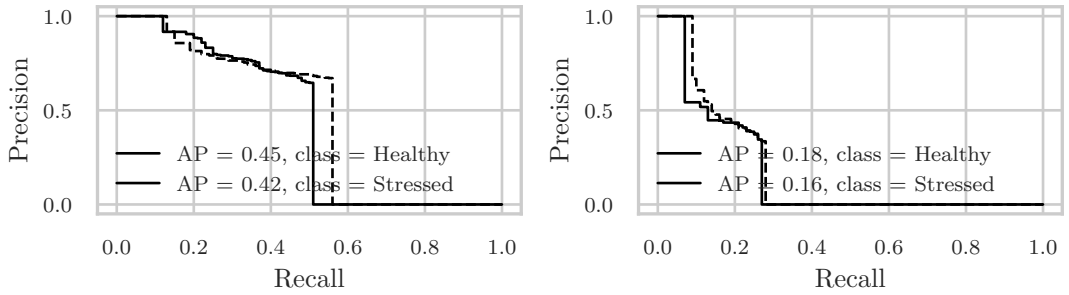


Figure 4.14: Precision-recall curves for IOU thresholds of 0.5 and 0.95. The AP of a specific threshold is defined as the area under the precision-recall curve of that threshold. The mAP across IOU thresholds from 0.5 to 0.95 in 0.05 steps  $\text{mAP}@0.5:0.95$  is 0.3581.

	precision	recall	f1-score	support
Healthy	0.711	0.555	0.623	766
Stressed	0.570	0.623	0.596	494
micro avg	0.644	0.582	0.611	1260
macro avg	0.641	0.589	0.609	1260
weighted avg	0.656	0.582	0.612	1260

Table 4.6: Precision, recall and F1-score for the optimized aggregate model.

### 4.3.2 Optimized Model

So far the metrics shown in table 4.5 are obtained with the non-optimized versions of both the object detection and classification model. Hyper-parameter optimization of the classifier led to significant model improvements, while the object detector has improved precision but lower recall and slightly lower mAP values. To evaluate the final aggregate model which consists of the individual optimized models, we run the same test described in section 4.3.

Table 4.6 shows precision, recall and F1-score for the optimized model on the same test dataset of 640 images. All of the metrics are better for the optimized model. In particular, precision for the healthy class could be improved significantly while recall remains at the same level. This results in a better F1-score for the healthy class. Precision for the stressed class is lower with the optimized model, but recall is significantly higher (0.502 vs. 0.623). The higher recall results in a 3% gain for the F1-score in the stressed class. Overall, precision is the same but recall has improved significantly, which also results in a noticeable improvement for the average F1-score across both classes.

Figure 4.15 confirms the performance increase of the optimized model established in table 4.6. The  $\text{mAP}@0.5$  is higher for both classes, indicating that the model better detects plants in general. The  $\text{mAP}@0.95$  is slightly lower for the healthy class, which means that the confidence for the healthy class is slightly lower compared to the non-optimized

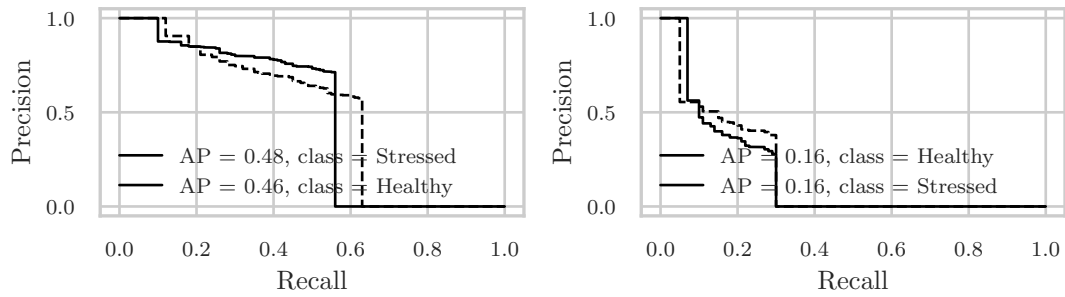


Figure 4.15: Precision-recall curves for IOU thresholds of 0.5 and 0.95. The AP of a specific threshold is defined as the area under the precision-recall curve of that threshold. The mAP across IOU thresholds from 0.5 to 0.95 in 0.05 steps  $\text{mAP}@0.5:0.95$  is 0.3838.

model. The result is that more plants are correctly detected and classified overall, but the confidence scores tend to be lower with the optimized model. The  $\text{mAP}@0.5:0.95$  could be improved by about 0.025.



# List of Figures

1.1	Setup in the field for water stress classification. . . . .	4
4.1	Object detection fitness per epoch. . . . .	12
4.2	Object detection precision and recall during training. . . . .	13
4.3	Object detection box and object loss. . . . .	14
4.4	Object detection AP@0.5 and AP@0.95. . . . .	15
4.5	Optimized object detection fitness per epoch. . . . .	16
4.6	Hyper-parameter optimized object detection precision and recall during training. . . . .	16
4.7	Hyper-parameter optimized object detection box and object loss. . . . .	17
4.8	Hyper-parameter optimized object detection AP@0.5 and AP@0.95. . . . .	18
4.9	Classifier accuracy and loss during training. . . . .	19
4.10	Classifier hyper-parameter optimization results. . . . .	20
4.11	Mean ROC and variability of hyper-parameter-optimized model. . . . .	21
4.12	F1-score of stratified 10-fold cross validation. . . . .	23
4.13	Classifier CAMs. . . . .	24
4.14	Aggregate model AP@0.5 and AP@0.95. . . . .	26
4.15	Optimized aggregate model AP@0.5 and AP@0.95. . . . .	27



## List of Tables

4.1	Precision, recall and F1-score for the object detection model. . . . .	14
4.2	Precision, recall and F1-score for the optimized object detection model. . . . .	17
4.3	Hyper-parameters and their possible values during optimization. . . . .	19
4.4	Hyper-parameters for the optimized classifier. . . . .	22
4.5	Precision, recall and F1-score for the aggregate model. . . . .	25
4.6	Precision, recall and F1-score for the optimized aggregate model. . . . .	26



## List of Algorithms



# Acronyms

**AP** Average Precision. 4, 5, 8

**CAM** Class Activation Mapping. 6, 9

**CNN** Convolutional Neural Network. 6

**Grad-CAM** Gradient-weighted Class Activation Mapping. 1, 6

**IOU** Intersection over Union. 4, 5, 8

**mAP** mean average precision. 4, 5, 8

**OID** Open Images Dataset. 1, 2

**ResNet** Residual Neural Network. 4, 5

**XAI** Explainable Artificial Intelligence. 1, 6



# Bibliography

[AH22] Omar El Ariss and Kaoning Hu. ResNet-based Parkinson’s Disease Classification. *IEEE Transactions on Artificial Intelligence*:1–11, 2022. doi: 10.1109/TAI.2022.3193651.

[AKG20] Shiva Azimi, Taranjit Kaur, and Tapan K Gandhi. Water Stress Identification in Chickpea Plant Shoot Images using Deep Learning. In *2020 IEEE 17th India Council International Conference (INDICON)*. 2020 IEEE 17th India Council International Conference (INDICON), pages 1–7, December 2020. doi: 10.1109/INDICON49873.2020.9342388.

[ALL<sup>+</sup>19] Jiangyong An, Wanyi Li, Maosong Li, Sanrong Cui, and Huanran Yue. Identification and Classification of Maize Drought Stress Using Deep Convolutional Neural Network. *Symmetry*, 11(2):256, 2, February 2019. doi: 10.3390/sym11020256. (Visited on 09/28/2022).

[Awa19] Mohamad M. Awad. Toward Precision in Crop Yield Estimation Using Remote Sensing and Optimization Techniques. *Agriculture*, 9(3):54, 3, March 2019. doi: 10.3390/agriculture9030054. (Visited on 10/18/2022).

[AWG21] Shiva Azimi, Rohan Wadhawan, and Tapan K. Gandhi. Intelligent Monitoring of Stress Induced by Water Deficiency in Plants Using Deep Learning. *IEEE Transactions on Instrumentation and Measurement*, 70:1–13, 2021. doi: 10.1109/TIM.2021.3111994.

[BB12] James Bergstra and Yoshua Bengio. Random search for hyper-parameter optimization. *The Journal of Machine Learning Research*, 13:281–305, null, February 1, 2012.

[BMR<sup>+</sup>20] Tom B. Brown, Benjamin Mann, Nick Ryder, Melanie Subbiah, Jared Kaplan, Prafulla Dhariwal, Arvind Neelakantan, Pranav Shyam, Girish Sastry, Amanda Askell, Sandhini Agarwal, Ariel Herbert-Voss, Gretchen Krueger, Tom Henighan, Rewon Child, Aditya Ramesh, Daniel M. Ziegler, Jeffrey Wu, Clemens Winter, Christopher Hesse, Mark Chen, Eric Sigler, Mateusz Litwin, Scott Gray, Benjamin Chess, Jack Clark, Christopher Berner, Sam McCandlish, Alec Radford, Ilya Sutskever, and Dario Amodei. Language Models are Few-Shot Learners. July 22, 2020. doi: 10.48550/arXiv.2005.14165. (Visited on 10/18/2022). preprint.

[BTD<sup>+</sup>21] Lefteris Benos, Aristotelis C. Tagarakis, Georgios Dolias, Remigio Berruto, Dimitrios Kateris, and Dionysis Bochtis. Machine Learning in Agriculture: A Comprehensive Updated Review. *Sensors*, 21(11):3758, 11, January 2021. DOI: 10.3390/s21113758. (Visited on 10/05/2022).

[BWL20] Alexey Bochkovskiy, Chien-Yao Wang, and Hong-Yuan Mark Liao. YOLOv4: Optimal Speed and Accuracy of Object Detection. April 22, 2020. DOI: 10.48550/arXiv.2004.10934. (Visited on 10/18/2022). preprint.

[CCR<sup>+</sup>21] Narendra Singh Chandel, Subir Kumar Chakraborty, Yogesh Anand Rajwade, Kumkum Dubey, Mukesh K. Tiwari, and Dilip Jat. Identifying crop water stress using deep learning models. *Neural Computing and Applications*, 33(10):5353–5367, May 1, 2021. DOI: 10.1007/s00521-020-05325-4. (Visited on 09/28/2022).

[DDS<sup>+</sup>09] Jia Deng, Wei Dong, Richard Socher, Li-Jia Li, Kai Li, and Li Fei-Fei. ImageNet: A large-scale hierarchical image database. In *2009 IEEE Conference on Computer Vision and Pattern Recognition*. 2009 IEEE Conference on Computer Vision and Pattern Recognition, pages 248–255, June 2009. DOI: 10.1109/CVPR.2009.5206848.

[HZR<sup>+</sup>16] Kaiming He, Xiangyu Zhang, Shaoqing Ren, and Jian Sun. Deep Residual Learning for Image Recognition. In *2016 IEEE Conference on Computer Vision and Pattern Recognition (CVPR)*. 2016 IEEE Conference on Computer Vision and Pattern Recognition (CVPR), pages 770–778, June 2016. DOI: 10.1109/CVPR.2016.90.

[JCS<sup>+</sup>22] Glenn Jocher, Ayush Chaurasia, Alex Stoken, Jirka Borovec, NanoCode012, Yonghye Kwon, Kalen Michael, TaoXie, Jiacong Fang, imyhxy, Lorna, Zeng Yifu, Colin Wong, Abhiram V, Diego Montes, Zhiqiang Wang, Cristi Fati, Jebastin Nadar, Laughing, UnglvKitDe, Victor Sonck, tkianai, yxNONG, Piotr Skalski, Adam Hogan, Dhruv Nair, Max Strobel, and Mrinal Jain. Ultralytics/yolov5: v7.0 - YOLOv5 SOTA Realtime Instance Segmentation, Zenodo, November 22, 2022. DOI: 10.5281/zenodo.7347926. (Visited on 07/30/2023).

[KB17] Diederik P. Kingma and Jimmy Ba. Adam: A Method for Stochastic Optimization. January 29, 2017. DOI: 10.48550/arXiv.1412.6980. (Visited on 04/05/2023). preprint.

[KRA<sup>+</sup>20] Alina Kuznetsova, Hassan Rom, Neil Alldrin, Jasper Uijlings, Ivan Krasin, Jordi Pont-Tuset, Shahab Kamali, Stefan Popov, Matteo Malloci, Alexander Kolesnikov, Tom Duerig, and Vittorio Ferrari. The Open Images Dataset V4: Unified image classification, object detection, and visual relationship detection at scale. *International Journal of Computer Vision*, 128(7):1956–1981, July 2020. DOI: 10.1007/s11263-020-01316-z. (Visited on 02/26/2023).

[LIM<sup>+</sup>22] Patricia López-García, Diego Intrigliolo, Miguel A. Moreno, Alejandro Martínez-Moreno, José Fernando Ortega, Eva Pilar Pérez-Álvarez, and Rocío Ballesteros. Machine Learning-Based Processing of Multispectral and RGB UAV Imagery for the Multitemporal Monitoring of Vineyard Water Status. *Agronomy*, 12(9):2122, 9, September 2022. doi: 10.3390/agronomy12092122. (Visited on 10/16/2022).

[LMB<sup>+</sup>15] Tsung-Yi Lin, Michael Maire, Serge Belongie, Lubomir Bourdev, Ross Girshick, James Hays, Pietro Perona, Deva Ramanan, C. Lawrence Zitnick, and Piotr Dollár. Microsoft COCO: Common Objects in Context. February 20, 2015. doi: 10.48550/arXiv.1405.0312. (Visited on 02/28/2023). preprint.

[MWL22] Patrick McEnroe, Shen Wang, and Madhusanka Liyanage. A Survey on the Convergence of Edge Computing and AI for UAVs: Opportunities and Challenges. *IEEE Internet of Things Journal*, 9(17):15435–15459, September 2022. doi: 10.1109/JIOT.2022.3176400.

[RRL<sup>+</sup>20] Paula Ramos-Giraldo, Chris Reberg-Horton, Anna M. Locke, Steven Mirsky, and Edgar Lobaton. Drought Stress Detection Using Low-Cost Computer Vision Systems and Machine Learning Techniques. *IT Professional*, 22(3):27–29, May 2020. doi: 10.1109/MITP.2020.2986103.

[RRM<sup>+</sup>20] Paula Ramos-Giraldo, S. Chris Reberg-Horton, Steven Mirsky, Edgar Lobaton, Anna M. Locke, Esleyther Henriquez, Ane Zuniga, and Artem Minin. Low-cost Smart Camera System for Water Stress Detection in Crops. In *2020 IEEE SENSORS*. 2020 IEEE SENSORS, pages 1–4, October 2020. doi: 10.1109/SENSORS47125.2020.9278744.

[SCD<sup>+</sup>20] Ramprasaath R. Selvaraju, Michael Cogswell, Abhishek Das, Ramakrishna Vedantam, Devi Parikh, and Dhruv Batra. Grad-CAM: Visual Explanations from Deep Networks via Gradient-based Localization. *International Journal of Computer Vision*, 128(2):336–359, February 2020. doi: 10.1007/s11263-019-01228-7. (Visited on 03/08/2023).

[SCL<sup>+</sup>20] Jinya Su, Matthew Coombes, Cunjia Liu, Yongchao Zhu, Xingyang Song, Shibo Fang, Lei Guo, and Wen-Hua Chen. Machine Learning-Based Crop Drought Mapping System by UAV Remote Sensing RGB Imagery. *Unmanned Systems*, 08(01):71–83, January 2020. doi: 10.1142/S2301385020500053. (Visited on 10/16/2022).

[WBL22] Chien-Yao Wang, Alexey Bochkovskiy, and Hong-Yuan Mark Liao. YOLOv7: Trainable bag-of-freebies sets new state-of-the-art for real-time object detectors. July 6, 2022. doi: 10.48550/arXiv.2207.02696. (Visited on 07/30/2023). preprint.

[ZHT22] Yiwei Zhong, Baojin Huang, and Chaowei Tang. Classification of Cassava Leaf Disease Based on a Non-Balanced Dataset Using Transformer-Embedded ResNet. *Agriculture*, 12(9):1360, 9, September 2022. doi: 10.3390/agriculture12091360. (Visited on 10/18/2022).

[ZKL<sup>+</sup>15] Bolei Zhou, Aditya Khosla, Agata Lapedriza, Aude Oliva, and Antonio Torralba. Learning Deep Features for Discriminative Localization. December 13, 2015. doi: 10.48550/arXiv.1512.04150. (Visited on 03/08/2023). preprint.

[ZWJ<sup>+</sup>17] Shuo Zhuang, Ping Wang, Boran Jiang, Maosong Li, and Zhihong Gong. Early detection of water stress in maize based on digital images. *Computers and Electronics in Agriculture*, 140:461–468, August 1, 2017. doi: 10.1016/j.compag.2017.06.022. (Visited on 10/16/2022).